HHS Public Access

Author manuscript

Magn Reson Med. Author manuscript; available in PMC 2024 October 01.

Published in final edited form as:

Magn Reson Med. 2023 October ; 90(4): 1555–1568. doi:10.1002/mrm.29712.

Establishing a hemoglobin adjustment for ^{129}Xe gas exchange MRI and MRS

Aryil Bechtel[1], **Junlan Lu**[2], **David Mummy**[1], **Elianna Bier**[3], **Suphachart Leewiwatwong**[3], **John Mugler III**[4], **Sakib Kabir**[1], **Alex Church**[1], **Bastiaan Driehuys**[1,2,3]

[1]Radiology, Duke University Medical Center, Durham, North Carolina, United States,

[2]Medical Physics Graduate Program, Duke University, Durham, North Carolina,

[3]Biomedical Engineering, Duke University, Durham, North Carolina, United States,

[4]Radiology and Medical Imaging, University of Virginia, Charlottesville, Virginia

Abstract

Purpose: ^{129}Xe MRI and MRS signals from airspaces, membrane tissues (M), and red blood cells (RBCs) provide measurements of pulmonary gas exchange. However, ^{129}Xe MRI/MRS studies have yet to account for hemoglobin concentration (Hb), which is expected to affect the uptake of ^{129}Xe in the membrane and RBC compartments. We propose a framework to adjust the membrane and RBC signals for Hb and use this to assess sex-specific differences in RBC/M and establish a Hb-adjusted healthy reference range for the RBC/M ratio.

Methods: We combined the 1-dimensional model of xenon gas exchange (MOXE) with the principle of TR-flip angle equivalence to establish scaling factors that normalize the dissolved-phase signals with respect to a standard Hb^0 (14 g/dL). ^{129}Xe MRI/MRS data from a healthy, young cohort (n=18, age=25.0±3.4 yrs) were used to validate this model and assess the impact of Hb adjustment on M/gas and RBC/gas images and RBC/M.

Results: Adjusting for Hb caused RBC/M to change by up to 20% in healthy individuals with normal Hb and had marked impacts on M/gas and RBC/gas distributions in 3D gas-exchange maps. RBC/M was higher in males than females both before and after Hb adjustment ($p<0.001$). Post Hb adjustment, the healthy reference value for RBC/M for a consortium-recommended acquisition of TR=15 ms and flip=20° was 0.589±0.083 (mean±SD).

Conclusion: MOXE provides a useful framework for evaluating the Hb dependence of the membrane and RBC signals. This work indicates that adjusting for Hb is essential for accurately assessing ^{129}Xe gas-exchange MRI/MRS metrics.

Keywords

Hyperpolarized ^{129}Xe MRI

Corresponding Author: Bastiaan Driehuys, Department of Radiology, Box 3302, Duke University Medical Center, Durham, NC 27710, Phone (919) 684-7786, Fax (919) 684-7158, bastiaan.driehuys@duke.edu.

1. Introduction

Hyperpolarized (HP) ^{129}Xe MRI and MRS have emerged as valuable ways of measuring regional pulmonary gas exchange function non-invasively and without the use of ionizing radiation[1–6]. When HP ^{129}Xe gas is inhaled, it freely diffuses from the airspaces, through the alveolar-capillary interstitial membrane, and into the capillary blood. In each of these individual compartments, the ^{129}Xe gas undergoes a distinct chemical shift, and can thus be quantified separately into MR signals from the airspace, interstitial membrane tissue (M), and red blood cells (RBCs). The latter two comprise the dissolved-phase signal. Through ^{129}Xe MRS, we can measure the aggregate signals from each of these three individual components, providing global measurements of lung function[7]. This framework can be extended to three-dimensional (3D) imaging, allowing us to visualize specific regions of ventilation and gas exchange abnormalities[8]. Ultimately, ^{129}Xe MRI provides spatially resolved estimates of the constituents of the diffusing capacity for carbon monoxide (DL_{CO}), a metric of gas exchange that is currently the most comprehensive standard physiological measurement of lung function[8].

^{129}Xe MRI and MRS have been used to characterize a range of pulmonary diseases, including chronic obstructive pulmonary disease (COPD), idiopathic pulmonary fibrosis (IPF), cystic fibrosis (CF), asthma, nonspecific interstitial pneumonia (NSIP), and pulmonary hypertension (PH)[1,8–10]. Within individual research sites, the ratio of RBC to membrane signal (RBC/M) has emerged as one of the most repeatable ^{129}Xe gas exchange metrics and appears to be a highly sensitive metric of gas exchange impairment in IPF patients[8,11].

To date, however, the RBC/M values reported by different research groups for healthy subjects still exhibit significant heterogeneity[6,12–16]. This is due in part to variable recruitment of reference cohorts, different acquisition parameters, and varying curve-fitting techniques used in calculating the measurement. An additional source of variance in RBC/M, which has yet to be addressed, is individual hemoglobin concentration (Hb). Indeed, the effects of Hb are not a unique problem to ^{129}Xe MRI. Hb is known to affect DL_{CO} measurements, which has led to the development of numerous adjustment approaches[17]. Given that the ^{129}Xe signal in RBCs is known to arise from transient interactions of ^{129}Xe with hemoglobin molecules[18], we expect subjects with high Hb to exhibit increased RBC signals relative to those with lower Hb. As a result, changes in Hb across subjects and in the same subject over time could mask differences in gas exchange function. Moreover, since males tend to have higher Hb than females, adjusting for Hb is also essential to examining sex differences[19]. Thus, it is necessary to adjust for the effect of Hb on ^{129}Xe dissolved-phase signals in order to more accurately measure underlying gas exchange function and to establish more accurate reference values for membrane uptake and RBC transfer imaging, as well as the global RBC/M ratio. We approach this problem by using the model of xenon gas exchange (MOXE) and the principle of TR-flip angle equivalence to estimate how the dissolved phase signals vary with Hb[20,21]. In addition to examining the sensitivity of the adjustment factors to physiological parameters, we assess their impact on gas-exchange images and the RBC/M ratio, examine sex-specific differences

in Hb-adjusted RBC/M values, and establish a Hb-adjusted reference value and range for young healthy adult subjects.

2. Methods

2.1 Model of xenon gas exchange (MOXE)

The effects of Hb on ^{129}Xe gas exchange can be investigated through the model of xenon gas exchange (MOXE) developed by Chang[20]. MOXE describes the short-term (~10 to 900 ms) recovery of the dissolved-phase signals after applying a saturating 90° radiofrequency (RF) pulse. This type of spectroscopy, known as chemical shift saturation recovery (CSSR), has been used in conjunction with MOXE to extract key physiological parameters, including hematocrit (Hct), alveolar surface area to volume ratio (S_A/V_g), air-blood membrane width (δ), total alveolar septal width (d), and pulmonary capillary transit time (t_x)[15,20,22]. The model assumes a 1D symmetric alveolar septum (Figure 1) and uses the 1D diffusion equation to describe the penetration of polarized ^{129}Xe from the airspaces into the alveolar septum. After integrating the solution over the air-blood membrane and capillary and accounting for blood flow, MOXE yields expressions for the signal in the air-blood membranes (S_{d1}) and total capillary blood (S_{d2}):

$$S_{d1}(t) = \frac{\lambda d}{2}\frac{S_A}{V_g}\left[\frac{2\delta}{d} - \frac{8}{\pi^2}\sum_{n=odd}\frac{1}{n^2}\left(1-\cos\left(\frac{n\pi\delta}{d}\right)\right)e^{-n^2t/T}\right] \quad [1]$$

$$S_{d2}(t) = \frac{\lambda d}{2}\frac{S_A}{V_g}\left\{2\left[\left(1-\frac{2\delta}{d}\right)\frac{t}{t_X} - \frac{8T}{\pi^2 t_X}\sum_{n=odd}\frac{1}{n^4}\cos\left(\frac{n\pi\delta}{d}\right)\left(1-e^{-n^2t/T}\right)\right]\right.$$
$$\left. + \left(1-\frac{t}{t_X}\right)\left[\left(1-\frac{2\delta}{d}\right) - \frac{8}{\pi^2}\sum_{n=odd}\frac{1}{n^2}\cos\left(\frac{n\pi\delta}{d}\right)e^{-n^2t/T}\right]\right\} \quad [2]$$

where λ is the Ostwald solubility of xenon in lung parenchyma and T is the xenon-exchange time constant: $T = d^2/\pi^2 D$. Here, D is the diffusion coefficient of dissolved xenon.

Finally, the membrane (S_M) and RBC (S_{RBC}) signals are constructed from S_{d1} and S_{d2} using η, the fraction of xenon in total blood interacting with RBCs.

$$S_{RBC}(t) = \eta S_{d2}(t) \quad [3]$$

$$S_M(t) = S_{d1} + (1-\eta)S_{d2}(t) \quad [4]$$

η is related to Hct by the Ostwald solubility of xenon in RBCs (λ_{RBC}) and plasma (λ_P) and can be written as a function of Hb by a simple scaling factor of 2.953×10^{-2} dL/g[23]. We note that Hb is typically measured directly from a venous blood sample or with an optical finger sensor[24]. However, *in vivo* estimates in humans and dogs indicate that the regional Hct in the lungs is lower than that in the systemic veins at a ratio, h_r, of roughly 0.9[25,26], a phenomenon thought to be caused by the Fåhræus effect and plasma skimming[27]. Thus, we rescale our peripherally-measured Hb by h_r to yield:

$$\eta(Hb) = \frac{(aHb)\lambda_{RBC}}{(aHb)\lambda_{RBC} + \lambda_P(1-(aHb))} \quad [5]$$

where $a = h_r \cdot 2.953 \times 10^{-2}$ dL/g . All MOXE parameter values were taken from the current literature for healthy populations, as summarized in Table 1. We note that the value of 12 μm for total septal thickness is approximated in Vasilescu et al.[28] using data from Gehr et al.[29] and the average diameter of an erythrocyte[28]. Further, we parameterized air-blood membrane thickness using the arithmetic mean value. While diffusion resistance is driven by the harmonic mean, the arithmetic mean is recognized to be more relevant to oxygen consumption and thus, analogously for ^{129}Xe membrane uptake[30].

The standard MOXE model is intended to capture dissolved-phase signal recovery as a function of the repetition time (TR), assuming application of 90° dissolved-phase flip angles[20]. However, typical ^{129}Xe gas-exchange MRI/MRS acquisitions use a dissolved-phase flip angle of 20[7]. We therefore model the steady-state magnetization for such acquisitions by using the principle of TR-flip angle equivalence, where, for a given TR and flip angle $\alpha < 90°$ [21,31]:

$$TR_{90} = \frac{TR}{1-\cos\ \alpha} \quad [6]$$

Here, TR_{90} is the TR that, when used with a 90° flip angle, yields the equivalent recovery as the TR and flip angle combination of interest. We note that while Eq. 6 breaks down as α approaches 90°, this effect has been shown to be relatively small in practice[21].

2.2 Deriving the Hb adjustment factors

At a fixed time $t = TR_{90}$, Hb adjustment scaling factors (Z) for both the membrane and RBC compartments were determined by the ratio of the corresponding dissolved-phase signals at a standardized Hb (Hb^0) to the signals at a subject's measured Hb (Hb). Due to the relatively long exchange times used in this work (TR≥15 ms), S_{d1} and S_{d2} can be approximated in the scaling factor relationships by dropping the terms in the series summations. Thus, on this timescale, the adjustment factor equations can be written such that the dependence on δ/d, t_X, and TR_{90} is more discernible.

$$S_{d1} \approx \lambda\delta\frac{S_A}{V_g} \quad [7]$$

$$S_{d2}(t) \approx \frac{\lambda d}{2}\frac{S_A}{V_g}\left(1-\frac{2\delta}{d}\right)\left(1+\frac{t}{t_X}\right) \quad [8]$$

This yields the following adjustment factors for the membrane, RBC, and RBC/M signals:

$$Z_M(TR_{90}, Hb) = \frac{S_M\left(TR_{90}, \eta\left(Hb^0\right)\right)}{S_M(TR_{90}, \eta(Hb))} = \frac{\frac{S_{d1}(TR_{90})}{S_{d2}(TR_{90})} + \left(1 - \eta\left(Hb^0\right)\right)}{\frac{S_{d1}(TR_{90})}{S_{d2}(TR_{90})} + (1 - \eta(Hb))} \approx \frac{\frac{2\delta/d}{(1-2\delta/d)(1+TR_{90}/t_X)} + \left(1 - \eta\left(Hb^0\right)\right)}{\frac{2\delta/d}{(1-2\delta/d)(1+TR_{90}/t_X)} + (1 - \eta(Hb))} \quad [9]$$

$$Z_{RBC}(TR_{90}, Hb) = \frac{S_{RBC}\left(TR_{90}, \eta\left(Hb^0\right)\right)}{S_{RBC}(TR_{90}, \eta(Hb))} = \frac{\eta\left(Hb^0\right)}{\eta(Hb)} \quad [10]$$

$$Z_{RBC/M}(TR_{90}, Hb) = \frac{Z_{RBC}(Hb)}{Z_M(TR_{90}, Hb)} \quad [11]$$

For the purposes of this study, we set Hb^0=14 g/dL, which was determined by averaging the healthy literature values for males (14.6 g/dL) and females (13.4 g/dL)[19]. Some insights into these factors can be gleaned in the limiting case of ignoring blood flow in Eq. 8 ($t/t_X \to 0$), in which case these Hb adjustment factor relationships reduce to a simple 1D model of the septum in which the signal from each compartment is proportional to its thickness and η simply provides the contributions of S_{d2} to the membrane and RBC resonances. However, in this work we opt to retain the blood flow term in Eq. 8 to provide a more complete treatment of Hb dependency at different TRs[20]. For estimating the RBC/M signal at different values of TR and Hb, S_{d1} and S_{d2} were approximated by using the first five terms of the series in Eqs. 1 and 2. Thus, the decay time constant (T/n^2) associated with the fifth term (n = 9) in each summation is <1 ms, which is well below the shortest recovery time examined in this study (TR_{90}~249 ms) and ensures sufficient precision in modeling the signal dynamics[20].

For ease of display, we will write Eqs. 9 and 10 in terms of the patient-specific Hb, the reference Hb^0, and in terms of the simplified expressions, R_1 (dimensionless), M_1(dL/g), and $M_2(TR_{90})$(dL/g):

$$Z_M(Hb) = \frac{1 + M_1 Hb}{1 + M_1 Hb^0 - M_2\left(TR_{90}\right) \bullet \left(Hb^0 - Hb\right)} \quad [12]$$

$$Z_{RBC}(Hb) = R_1 + \frac{Hb^0(1 - R_1)}{Hb} \quad [13]$$

$$R_1 = \eta\left(Hb^0\right)\left(1 - \frac{\lambda_P}{\lambda_{RBC}}\right) \quad [14]$$

$$M_1 = a\left(\frac{\lambda_{RBC}}{\lambda_P} - 1\right) \quad [15]$$

$$M_2(TR_{90}) = \frac{\left(\frac{2\delta/d}{(1-2\delta/d)(1+TR_{90}/t_X)}M_1 - a\right)}{\left(\frac{2\delta/d}{(1-2\delta/d)(1+TR_{90}/t_X)} + \frac{\lambda_P\left(1-aHb^0\right)}{aHb^0\lambda_{RBC} + \lambda_P\left(1-aHb^0\right)}\right)} \quad [16]$$

The adjustment factors for the membrane signal and RBC/M ratio were determined using approximate literature values for δ/d and t_x. However, we also conducted a sensitivity analysis to determine the effect of these parameters on Z_M and $Z_{RBC/M}$ by allowing each parameter to vary, while holding the remaining variables fixed according to Table 1. A sensitivity analysis was also conducted to assess the effect of h_r on Z_{RBC}, Z_M, and $Z_{RBC/M}$, as experiments with artificial microvascular networks suggest that the amount of reduction of Hct in small vessels may depend on the feeding Hct and perfusion pressure[27]. We note that adjustment factors are independent of S_A/V_g, which was therefore not included in the sensitivity analysis. We also note that membrane and RBC/M adjustment factors are dependent on TR_{90} and therefore specific to the TR-flip angle combination used.

2.3 Correcting for unequal RF excitation

The current ^{129}Xe MRI clinical trials consortium standard for gas-exchange MRI/MRS applies RF excitation at the RBC chemical shift of 218 ppm[7]. However, this disproportionately amplifies the RBC signal relative to the 198-ppm membrane signal. We sought to obtain a more accurate measure of the RBC/M ratio by considering the scenario of equal excitation centered at 208 ppm between the two resonances. To determine a theoretical scaling factor that captures the difference between 218- and 208-ppm excitation, a Hanning-windowed 0.69 ms sinc RF pulse was simulated at both frequencies using the Bloch equations in MATLAB by applying a series of rotations about the time-varying B_1 vector. The relative strength of signal at the membrane and RBC resonances was then visualized by plotting the distribution of transverse magnetization (M_{xy}) over frequency. The theoretical result was then compared with a scaling factor empirically determined from RBC/M values measured at both frequencies.

2.4 Human subjects

Study protocols were approved by the Institutional Review Board of Duke University Medical Center. The primary cohort for this work consisted of 22 healthy volunteers between 18 and 30 years old (age=25.3±3.4 yrs, 8 female). All subjects provided written and informed consent prior to participation. Subjects had no cardiac arrhythmias, <5 pack-years of smoking, no tobacco use in the last 5 years, no history of using other inhaled products more than once per week in the past year, had never been diagnosed with a pulmonary disorder, had no respiratory illness within 30 days of their scan, and were not pregnant or lactating. All subjects underwent DL_{CO} measurement, spirometry, and non-invasive Hb measurement with a point of care optical finger sensor (Masimo Pronto, Irvine, CA, USA). All subjects were scanned according to the recommended protocols for ^{129}Xe gas-exchange MRI/MRS outlined in Niedbalski et al., with the exception that several MRS scans were done at different TRs (15 ms (n=10 subjects, four of whom were later excluded), 20 ms

(n=12), and 73 ms (n=4))[7]. We note that the number of subjects scanned at each TR does not add up to the 22 unique subjects in our sample because four subjects were scanned at both TR=20 and 73 ms. Two subjects were excluded because their measured K_{CO}, FVC (forced vital capacity), or FEV1(forced expiratory volume in one second) was less than 80% of the value predicted by the Global Lung Function Initiative (GLI)[32]. Two subjects had an FEV1 79% of predicted but were included because their ventilation MRI exhibited no defects. An additional subject was excluded due to insufficient signal in the Hb sensor and another due to abnormal gas-exchange MRI that was attributed to a subsequent neurofibromatosis diagnosis. This left a final sample of 18 subjects (age=25.0±3.4 yrs, 6 female).

A secondary cohort of healthy volunteers with a broader age range (n=19, age=40.2±15.2, 8 female) underwent standard ^{129}Xe gas-exchange MRS[7] with RF excitation pulses centered at both 208 and 218 ppm, with the order of the two scans randomized for each subject. While current protocol recommendations use 218-ppm excitation (at the RBC resonance)[7], future protocols may use excitation at 208 ppm (directly between the RBC and membrane resonances). This sample was used to empirically measure the ratio of RBC/M values obtained when using RF excitation centered at 208 ppm vs 218 ppm. Two subjects were included in both the primary and secondary cohorts.

2.5 Acquisition and image processing

2.5.1 ^{129}Xe spectroscopy—All spectra and images were acquired at 3 Tesla. Subjects inhaled HP ^{129}Xe and spectra were acquired during a 10–16 second breath-hold[6]. Gas- and dissolved-phase ^{129}Xe were excited using 0.69 ms Hanning-windowed sinc-shaped RF pulses applied at frequencies corresponding to the ^{129}Xe gas chemical shift of 0 ppm and to the RBC chemical shift of 218 ppm (or at 208 ppm for the secondary cohort), respectively. Free induction decays (FIDs) (n=200 to 600) were acquired at a target dissolved-phase flip angle of 20°, and TR of 15, 20, or 73 ms. The spectra from these FIDs were used to measure the strength of the RBC and membrane signals.

FIDs from the first 2 seconds of the breath-hold were discarded to remove signal that accumulated during inhalation in the larger vasculature, downstream of the pulmonary capillary bed[7]. FIDs from the next 1 second were averaged and fit, in the time domain, to Voigt and Lorentzian models, to calculate the areas of the membrane and RBC spectral peaks respectively. These areas were used to determine the RBC/M ratio[6]. These values were adjusted for Hb by multiplying by the RBC/M adjustment factor, $Z_{RBC/M}(TR_{90}, Hb)$, corresponding to the acquisition TR and Hb measured prior to the scan. To expand the TR=15 ms cohort, we included 12 subjects acquired at TR=20 ms, whose RBC/M ratios were decreased by a correction factor of 3% determined using the MOXE model to relate RBC/M ratios measured at these TRs. Data from this combined TR=15 ms and TR=20 ms cohort were used to compare the trend in measured RBC/M versus Hb to that predicted by MOXE as well as to calculate adjusted RBC/M reference values.

2.5.2 ^{129}Xe gas-exchange imaging—Gas exchange images were acquired during a 16-second breath-hold according to established protocols (TR=15 ms, dissolved flip angle=20°)[7]. Per the consortium standard, the dissolved-phase signals were decomposed

via the 1-point Dixon method, using non Hb-adjusted RBC/M values to produce images of gas, membrane, and RBC signal distributions[7]. Off-resonance gas-phase excitation was suppressed by tailoring a Hanning-windowed sinc-shaped RF pulse duration to keep the ratio of gas to dissolved-phase signal ratio <10%; the optimal duration was found to be 0.69 ms for 218-ppm excitation[33] and 0.71 ms for 208-ppm excitation. Ventilation maps were adjusted for B_1 inhomogeneity, segmented, and normalized according to established protocols[33]. Membrane and RBC images were further segmented to exclude regions of ventilation defect and then divided voxel-wise by the ventilation images, creating maps of membrane/gas (M/gas) and RBC/gas signal. To adjust these images for Hb, every voxel was multiplied by the appropriate membrane (Z_M) or RBC (Z_{RBC}) Hb adjustment scaling factor. The M/gas and RBC/gas images were then color binned as previously described into 6 and 8 bins (respectively), each of which represents one additional standard deviation away from the mean of a corresponding healthy reference distribution[34]. We note that the reference distributions used for these examples were not adjusted for Hb[35]. Images were quantified by recording the fraction (relative to the thoracic cavity volume) of voxels in the lowest bin, second lowest bin, and the 2 highest RBC/gas bins and 3 highest M/gas bins. Respectively, these are referred to as the “defect”, “low”, and “high” percentages.

3. Results

The primary cohort had the following pulmonary function values (mean±SD): FVC=101.5±7.8% predicted, FEV1=98.2±11.6% pred., FEV1/FVC=0.82±0.07, DL_{CO}=100.3±11.1% pred., and K_{CO}=104.7±9.5% pred. Mean Hb for the total sample was 14.0±1.6 g/dL (range: 10.2 to 16.5 g/dL) and was significantly higher in males (14.7±1.3 g/dL vs. 12.8±1.4 g/dL, $p<0.05$). For a Hb range of 7–19 g/dL and the TRs examined, the neglect of the series summation terms in Eqs. 1 and 2 resulted in <0.6% change in Hb adjustment factors. Figure 2 shows the calculated Hb adjustment curves for membrane, RBC, and RBC/M (Z_M, Z_{RBC}, and $Z_{RBC/M}$) for TR=15 ms and flip angle=20° acquisitions. As Hb increases, Z_{RBC} and $Z_{RBC/M}$ decrease while Z_M increases. Thus, for patients with $Hb < Hb^0$, application of the adjustment factors will increase the RBC signal while decreasing the membrane signal. For a typical healthy Hb range of 12 to 17 g/dL[36], adjustments can yield changes as large as 9% and 13% in membrane and RBC signal, respectively. Since alterations in Hb cause the membrane and RBC signals to move in opposite directions, these individual adjustment effects are compounded in the RBC/M ratio, which can change by up to 20% across this range. The effects are even larger for patients with anemia, who might exhibit Hb in the range of 7–12 g/dL. The RBC and RBC/M adjustment factor curves are also notably non-linear, causing 10% and 20% more change (respectively) for patients at the lower versus upper ranges of healthy Hb.

Figure 3 shows the distribution of ^{129}Xe transverse magnetization (M_{xy}) over frequency from simulations of 218- and 208-ppm Hanning-windowed sinc RF pulses. The distributions reveal that centering an RF pulse at 218 ppm causes the membrane signal to experience only 89% of the maximum excitation, whereas centering the pulse at 208 ppm causes the membrane and RBC components to be equally excited at 97% of the maximum. Collectively, the simulated RBC/M ratio decreases by a factor of 0.89 when using a 208-

versus 218-ppm excitation. We measured this factor empirically by scanning our secondary sample of subjects at both 208- and 218-ppm RF excitation, yielding an identical ratio of 0.89 with a standard deviation of ±0.11.

Figure 4A shows a plot of non Hb-adjusted RBC/M vs Hb for all subjects in the primary cohort after correcting for unequal excitation along with the Hb scaling curve calculated from the MOXE model. The dashed curves denote the predicted MOXE values ± the coefficient of repeatability (CR) for the RBC/M ratio, about 0.09[37]. Thus, for points that lie within the bounded region, the MOXE curve is within the expected range of repeatability. Figure 4B depicts the distribution of Hb-adjusted RBC/M values measured at TRs of 15, 20, and 73 ms after adjusting for unequal excitation along with the RBC/M modeled by MOXE at Hb^0=14 g/dL. In both plots, the MOXE curve provides a good approximation of the trend and scale of the data. These results suggest that MOXE provides a reasonable basis for estimating how RBC/M scales with Hb in healthy subjects.

Given that we have used fixed healthy reference parameters in MOXE to establish adjustment factors, we must also understand how these factors change in patients whose parameters vary from published healthy reference values. This is shown in Figure 5 where δ/d, t_x, and h_r were varied while all other variables were held constant according to the values in Table 1[28]. The figure shows that the membrane and RBC/M Hb adjustment factors are sensitive to changes in relative air-blood membrane thickness but robust to variation in t_x and h_r. Because the Hb adjustment factors are smaller when δ/d is larger, the proposed calculations may overestimate the required changes in patients with interstitial thickening. When applied to these patients, the proposed adjustment factors are accurate to within about ±8% for those within the typical Hb range, and about ±15% for those with abnormal Hb.

Figure 6 shows representative images of gas, membrane uptake, and RBC transfer after application of a thoracic cavity mask (A) for a healthy subject with Hb=10.2 g/dL and demonstrates the effect of applying the Hb adjustment factors to the 3D gas exchange maps of M/gas (B) and RBC/gas (C). Given the subject's relatively low Hb, applying the adjustments caused M/gas to decrease significantly in the left lung while RBC/gas visibly increases in the apex of the right lung and center of both lungs. These changes are also readily visualized in the histograms used to characterize the M/gas and RBC/gas distributions as well as in the effects on the quantitative defect, low, and high metrics for each. In this case, the high M/gas and low RBC/gas percentages decreased by 8–9% and the high RBC/gas percentage increased by 7%.

Figure 7 shows the distribution of RBC/M values for a standard TR=15 ms and 20° flip acquisition at 218-ppm excitation for all 18 healthy subjects before and after Hb adjustment. Data are differentiated by sex and lines connect unadjusted and adjusted values for the same subject. RBC/M was significantly higher in the male vs female samples both before adjustment (0.663±0.070 vs. 0.458±0.059, $p<0.0001$) and after (0.631±0.069 vs. 0.506±0.031, $p<0.001$). Prior to Hb-adjustment, the mean healthy RBC/M of the total sample was 0.594±0.118, which was slightly reduced by adjustment to 0.589; however, the standard deviation decreased by over 50% to ±0.083. Scaling this result to the scenario of equal dissolved-phase excitation (208 ppm), yields a reference RBC/M ratio of 0.525±0.074.

4. Discussion

In this work, the MOXE framework was used to evaluate the Hb dependence of dissolved-phase ^{129}Xe signals by allowing Hb to vary while other structural variables were fixed. This differs from the typical way in which MOXE is fit to CSSR curves in order to estimate these microstructural parameters as an average over the lungs. Here, we instead exploit the model's established ability to robustly recapitulate ^{129}Xe signal saturation and recovery[15,20,22,38–41] and use this capability as a framework for understanding the impact of Hb on consortium-adopted protocols for ^{129}Xe MRI/MRS[7]. While using MOXE with CSSR can provide information on lung structure, this latter approach is better suited toward connecting gas-exchange MRI/MRS to lung function in that it can be related to the constituents of DL_{CO}[8]. The model-predicted dependence of RBC/M on Hb matches the trend we observed in 18 healthy subjects. By combining the model with the principle of TR-flip angle equivalence, we established scaling factors to adjust the consortium-standard dissolved-phase signals relative to a standard Hb of 14 g/dL. We found that the proposed Hb adjustment can have a large impact on the RBC/M ratio and maps of M/gas and RBC/gas signal. Over a healthy Hb range, the shape of the RBC adjustment curve is similar to the curve for DL_{CO}[42]. However, the percentage change caused by the RBC and RBC/M factors is 1.7 and 2.7 times greater than that of DL_{CO}, respectively[42]. We note that it would also have been possible to estimate Hb dependencies from more straightforward correlation analysis. While this would have the advantage of requiring no underlying physiological model, it would have been limited in several ways. Without the use of a physiological model, the exact non-linearity of Hb dependence in the dissolved-phase signals would be difficult to infer from limited amounts of empirical data. Moreover, such correlation approaches would not be likely to highlight the potential effects of membrane thickness on the adjustment factors.

As illustrated by our healthy volunteer imaging, low Hb can result in regions of abnormally high M/gas signal, which are removed upon adjustment. Given the emergence of high M/gas as a biomarker for detecting the presence of interstitial lung disease (ILD)[10,43,44], it is imperative to avoid misdiagnoses due to non-pulmonary factors. In this case, we see that applying the Hb adjustment brings the M/gas map back into the normal range. RBC/M values from our sex-specific samples reveal how the Hb adjustment reduces, but does not eliminate, the difference in male and female values. This suggests that, while generally lower Hb in the female sample exacerbates the difference in unadjusted RBC/M distributions, there remains another underlying mechanism driving this disparity. This could reflect sex-specific differences in relative capillary blood volume or membrane tissue volume but could also be attributable to flaws in the study design. For example, our study used a mixture of fixed (1 liter) and tailored ^{129}Xe dose volumes across subjects. Given that females have generally lower thoracic cavity volumes, some may have been scanned at higher lung inflation[45]. Notably, RBC/M has been shown to be inversely correlated with inflation level[9,46,47].

We found that the Hb adjustment factors for membrane and RBC/M presented here are sensitive to changes in the ratio of air-blood membrane to total septal thickness. This is because the ratio changes the fraction of dissolved-phase signal originating from the

capillary. When the air-blood membranes are thicker (as in patients with ILD), this fraction is lower and the effect of Hb on RBC/M is reduced, particularly in the extremes of the Hb ranges. For patients with thickening of air-blood membranes, the proposed adjustment could be overestimated by up to ~8% for those in the extremes of the normal range of Hb and up to ~15% for those with abnormal values. However, the impact of Hb on the RBC signal itself is independent of alveolar septal thicknesses and thus Z_{RBC} represents a minimum required Hb adjustment for RBC/M.

It is instructive to compare our Hb-adjusted healthy reference RBC/M values with age-matched cohorts that have been reported in the literature (Table 2). Note that this Hb adjustment is distinct from the common practice of reporting PFTs as a percentage of a predicted reference value. The Hb adjustment here seeks to remove a confounding factor prior to forming a consolidated estimate of reference values for 18–30 yr old subjects. Here, we have again used the MOXE model and TR-flip angle equivalence to generate scaling factors to transform the literature data to the standardized TR=15 ms and flip=20° regime. The Bier et al.[6] data were also rescaled by 0.89 and the Grist et al.[48] data by 1/0.89 to account for unequal dissolved-phase excitation at 218 ppm and 198 ppm, respectively. As shown in the table, our 208-ppm reference RBC/M of 0.53±0.07 is in good agreement with prior literature values. In evaluating these comparisons, we note that Xie et al. did not consider DL_{CO} or K_{CO} in evaluating volunteer health, while Grist et al. and Bier et al. made no exclusions based on PFTs[6,16,48]. By contrast, the sample size presented here is significantly larger, contains a more even sex distribution, and was collected with stricter inclusion/exclusion criteria than the other three studies. Thus, in addition to considering Hb adjustment, our measurements arguably provide the most robust reference value for RBC/M available to date.

4.1 Limitations and next steps

The MOXE model captures the general shape of ^{129}Xe saturation and recovery curves and serves as a starting point for understanding the impact of Hb on the dissolved-phase signal. However, there remains some uncertainty regarding the accepted MOXE parameters even in healthy subjects. In several studies, the best-fit values for the Hct parameter are significantly lower than typical clinical reference values[15,20,22]. This could be the result of not accounting for reduced Hct in the pulmonary capillaries, the large number of interdependent fit parameters[15], and MOXE's inability to capture variance in tissue thickness and asymmetry about the capillaries[20,22,49]. In this work, the air-blood membrane thickness and total capillary width were based on cross-sections of histological samples that have an analogous geometry to the 1D design of MOXE. However, this representation of the alveolar capillaries greatly oversimplifies their more complex 3D mesh structure[50,51]. Furthermore, the ratios of air-blood membrane to capillary width often associated with MOXE are significantly lower than typical tissue to blood volume ratios measured in the lung[29,52,53]. There are several possible reasons for this discrepancy. Firstly, acquisition at a high flip angle and short TRs limits the diffusion of ^{129}Xe into distal structural tissues. Secondly, because the solubility of ^{129}Xe is unknown in some structures, such as collagen, there may be some tissues into which it does not readily diffuse. Finally, volumetric ratios in the 3D regime may be inherently incomparable to thickness ratios in a 1D projection

such as MOXE. This simplification of a complex 3D alveolar-capillary geometry could thus introduce bias into the way dissolved-phase ^{129}Xe signals appear to depend on Hb. The number of fit parameters in MOXE could be reduced by fixing those that can be estimated or measured through other means, such as Hb. Further, MOXE's simplistic 1D structure could be addressed by transitioning to 2D or 3D gas diffusion models that incorporate varying tissue thickness and asymmetric gas exchange on either side of the capillaries[49,54].

We also note limitations in our empirical validation of the proposed Hb dependence of RBC/M. Our comparison of MOXE to the observed trend in RBC/M vs Hb was limited by variation in RBC/M measurements. For two thirds of subjects, the MOXE curve fell within the expected range of repeatability, indicating that intra-patient variability could account for some of the variation in RBC/M. Variation between subjects could also be the result of using different dose volumes across subjects. However, a significant amount of variation is likely due to physiological differences between subjects. Thus, validation studies would benefit from scanning the same sample or subject before and after interventions that alter Hb, but not underlying pulmonary physiology. Notably, the Hb dependence from the RBC compartment could be evaluated by examining ^{129}Xe dissolved-phase signals in whole blood samples of varying Hb. Moreover, this could be complemented by in vivo validation such as scanning blood donors, whose Hb is expected to drop ~1 g/dL after donation[55]. More significant changes in Hb could be expected from anemic patients undergoing a blood transfusion, which can drive up Hb by 2–3 g/dL[56]. And finally, there is subset of subjects with hemochromatosis who regularly undergo therapeutic apheresis or phlebotomies that induce changes in Hb[57]. Given the dependence of the proposed adjustment factors on relative air-blood membrane thickness, such studies are particularly warranted in patients with interstitial lung disease.

Furthermore, while our Hb-adjusted RBC/M distributions measured at TRs of 15, 20, and 73 ms are in approximate agreement with MOXE, a more robust validation of the Hb-adjusted RBC/M vs. TR curve requires data at more exchange times. We also note that the deviation of the distribution at TR=73 ms from MOXE could be the result of a low sample size at that TR (n=4). A more appropriate validation method would be to apply a sequence of 20° RF pulses on a single subject with known Hb and measure the dissolved-phase signal recovery after different exchange times.

It is also important to note limitations in our healthy reference data and sample. All subjects were Hb-adjusted according to $Hb^0 = 14\text{g/dL}$, regardless of sex. However, because males tend to have higher Hb than females, sex-specific adjustment factors may be more appropriate[19]. Furthermore, the M/gas and RBC/gas reference distributions used to color bin our gas-exchange maps were built with unadjusted data. In future studies, new Hb-adjusted imaging reference distributions should be constructed. Finally, while our sample's age range of 18–30 yrs. gives insight into the upper range of healthy lung function, reference data should also be collected for older and younger age ranges. This will allow us to account for healthy, age-related changes in ^{129}Xe gas-exchange metrics, such as reductions in RBC/M with increased age[47,58]. Finally, we note that the use of two different TRs and both fixed and tailored dose volumes could introduce bias and variability into our resulting healthy reference distributions. While we attempted to mitigate bias between subjects scanned at

TR=15 ms and TR=20 ms by applying an adjustment factor, future reference data should be drawn from subjects scanned with the same acquisition parameters and tailored dose volumes.

5. Conclusion

In this work, we used the MOXE framework to estimate the dependence of ^{129}Xe dissolved-phase signals on Hb and showed that it is consistent with empirical RBC/M data from a young, healthy cohort. Our findings show that performing even the minimum required adjustments can result in significant changes in RBC transfer and RBC/M, and thus, adjusting ^{129}Xe gas-exchange MRI/MRS metrics for Hb is essential for accurately assessing lung function. This model can be used to establish Hb-adjustment factors that normalize M/gas, RBC/gas, and RBC/M measurements to a fixed reference Hb value, allowing for meaningful comparisons of Hb-independent lung function across patients or within the same patient. This approach will enable investigations of sex-driven differences in membrane uptake and RBC transfer, analysis of gas exchange MRI in patients with significant anemia (such as transplant patients), and the creation of Hb-adjusted healthy reference distributions.

Acknowledgements

We thank Matt Willmering for insights regarding 208- vs 218-ppm excitation.

Funding support:

NIH/NHLBI R01HL105643, R01HL126771, R01HL153641, R01HL153872, NSF GRFP DGE-1644868

References

1. Marshall H, Stewart NJ, Chan HF, Rao M, Norquay G, Wild JM. In vivo methods and applications of xenon-129 magnetic resonance. Prog Nucl Magn Reson Spectrosc. 2021;122:42–62. doi:10.1016/J.PNMRS.2020.11.002 [PubMed: 33632417]
2. Wang JM, Robertson SH, Wang Z, et al. Using hyperpolarized 129Xe MRI to quantify regional gas transfer in idiopathic pulmonary fibrosis. Thorax. 2018;73(1):21–28. doi:10.1136/THORAXJNL-2017-210070 [PubMed: 28860333]
3. Virgincar RS, Cleveland ZI, Sivaram Kaushik S, et al. Quantitative analysis of hyperpolarized 129Xe ventilation imaging in healthy volunteers and subjects with chronic obstructive pulmonary disease. NMR Biomed. 2013;26(4):424–435. doi:10.1002/NBM.2880 [PubMed: 23065808]
4. Thomen RP, Walkup LL, Roach DJ, Cleveland ZI, Clancy JP, Woods JC. Hyperpolarized 129Xe for investigation of mild cystic fibrosis lung disease in pediatric patients. J Cyst Fibros. 2017;16(2):275–282. doi:10.1016/J.JCF.2016.07.008 [PubMed: 27477942]
5. Wang Z, Bier EA, Swaminathan A, et al. Diverse cardiopulmonary diseases are associated with distinct xenon magnetic resonance imaging signatures. Eur Respir J. 2019;54(6). doi:10.1183/13993003.00831-2019
6. Bier EA, Robertson SH, Schrank GM, et al. A protocol for quantifying cardiogenic oscillations in dynamic 129 Xe gas exchange spectroscopy: The effects of idiopathic pulmonary fibrosis. NMR Biomed. 2019;32(1). doi:10.1002/NBM.4029
7. Niedbalski PJ, Hall CS, Castro M, et al. Protocols for multi-site trials using hyperpolarized 129Xe MRI for imaging of ventilation, alveolar-airspace size, and gas exchange: A position paper from the 129Xe MRI clinical trials consortium. Magn Reson Med. 2021;86(6):2966–2986. doi:10.1002/mrm.28985 [PubMed: 34478584]

8. Wang Z, Rankine L, Bier EA, et al. Using hyperpolarized 129Xe gas-exchange MRI to model the regional airspace, membrane, and capillary contributions to diffusing capacity. J Appl Physiol. 2021;130(5):1398–1409. doi:10.1152/japplphysiol.00702.2020 [PubMed: 33734831]
9. Qing K, Mugler JP, Altes TA, et al. Assessment of lung function in asthma and COPD using hyperpolarized 129Xe chemical shift saturation recovery spectroscopy and dissolved-phase MRI. NMR Biomed. 2014;27(12):1490–1501. doi:10.1002/nbm.3179 [PubMed: 25146558]
10. Mummy DG, Bier EA, Wang Z, et al. Hyperpolarized 129Xe MRI and spectroscopy of gas-exchange abnormalities in nonspecific interstitial pneumonia. Radiology. 2021;301(1):211–220. doi:10.1148/radiol.2021204149 [PubMed: 34313473]
11. Weatherley ND, Stewart NJ, Chan HF, et al. Hyperpolarised xenon magnetic resonance spectroscopy for the longitudinal assessment of changes in gas diffusion in IPF. Thorax. 2019;74(5):500–502. doi:10.1136/thoraxjnl-2018-211851 [PubMed: 30389827]
12. Hahn AD, Carey KJ, Barton GP, et al. Hyperpolarized 129 Xe MR Spectroscopy in the Lung Shows 1-year Reduced Function in Idiopathic Pulmonary Fibrosis. Radiology. Published online July 26, 2022. doi:10.1148/radiol.211433
13. Qing K, Mugler JP, Altes TA, et al. Assessment of lung function in asthma and COPD using hyperpolarized 129Xe chemical shift saturation recovery spectroscopy and dissolved-phase MRI. NMR Biomed. 2014;27(12):1490–1501. doi:10.1002/nbm.3179 [PubMed: 25146558]
14. Kaushik SS, Freeman MS, Yoon SW, et al. Measuring diffusion limitation with a perfusion-limited gas-Hyperpolarized Xe gas-transfer spectroscopy in patients with idiopathic pulmonary fibrosis. J Appl Physiol. 2014;117:577–585. doi:10.1152/japplphysiol.00326.2014.-Al [PubMed: 25038105]
15. Stewart NJ, Leung G, Norquay G, et al. Experimental Validation of the Hyperpolarized 129 Xe Chemical Shift Saturation Recovery Technique in Healthy Volunteers and Subjects with Interstitial Lung Disease. Magn Reson Med. 2015;74:196–207. doi:10.1002/mrm.25400 [PubMed: 25106025]
16. Xie J, Li H, Zhang H, et al. Single breath-hold measurement of pulmonary gas exchange and diffusion in humans with hyperpolarized 129Xe MR. NMR Biomed. 2019;32(5):e4068. doi:10.1002/NBM.4068 [PubMed: 30843292]
17. Marrades RM, Diaz O, Roca J, et al. Adjustment of DL(CO) for hemoglobin concentration. Am J Respir Crit Care Med. 1997;155(1):236–241. doi:10.1164/ajrccm.155.1.9001318 [PubMed: 9001318]
18. Bifone A, Song YQ, Seydoux R, et al. NMR of laser-polarized xenon in human blood. Proc Natl Acad Sci U S A. 1996;93(23):12932–12936. doi:10.1073/pnas.93.23.12932 [PubMed: 8917521]
19. Munkholm M, Marott JL, Bjerre-Kristensen L, et al. Reference equations for pulmonary diffusing capacity of carbon monoxide and nitric oxide in adult Caucasians. Eur Respir J. 2018;52(1). doi:10.1183/13993003.00677-2015
20. Chang Y v. MOXE: A model of gas exchange for hyperpolarized 129Xe magnetic resonance of the lung. Magn Reson Med. 2013;69(3):884–890. doi:10.1002/MRM.24304 [PubMed: 22565296]
21. Ruppert K, Amzajerdian F, Hamedani H, et al. Assessment of flip angle–TR equivalence for standardized dissolved-phase imaging of the lung with hyperpolarized 129Xe MRI. Magn Reson Med. 2019;81(3):1784–1794. doi:10.1002/MRM.27538 [PubMed: 30346083]
22. Chang Y v Quirk JD, Ruset IC Atkinson JJ, William Hersman F Woods JC. Quantification of Human Lung Structure and Physiology Using Hyperpolarized 129 Xe. Magn Reson Med. 2014;71:339–344. doi:10.1002/mrm.24992 [PubMed: 24155277]
23. Billett HH. Hemoglobin and Hematocrit. Anesthesiology. 1990;28(4):763–763. doi:10.1097/00000542-196707000-00028
24. Foster KE, Sahay RD, Zhang N, Hardie WD. Results of a prospective study evaluating a noninvasive method of hemoglobin adjustment for determining the diffusing capacity of the lung. Ann Am Thorac Soc. 2017;14(1):41–48. doi:10.1513/AnnalsATS.201603-197OC [PubMed: 27870589]
25. Brudin LH, Valind SO, Rhodes CG, Turton DR, Hughes JM. Regional lung hematocrit in humans using positron emission tomography. J Appl Physiol. 1986;60(4):1155–1163. doi:10.1152/JAPPL.1986.60.4.1155 [PubMed: 3486179]

26. Overholser KA, Lomangino NA, Harris TR, Bradléy JD, Bosan S. Deduction of pulmonary microvascular hematocrit from indicator dilution curves. Bull Math Biol. 1994;56(2):225–247. doi:10.1007/BF02460641 [PubMed: 8186753]
27. Reinhart WH, Piety NZ, Shevkoplyas SS. Influence of feeding hematocrit and perfusion pressure on hematocrit reduction (Fåhræus effect) in an artificial microvascular network. Microcirculation. 2017;24(8). doi:10.1111/MICC.12396
28. Vasilescu DM, Phillion AB, Kinose D, et al. Comprehensive stereological assessment of the human lung using multiresolution computed tomography. J Appl Physiol. 2020;128(6):1604–1616. doi:10.1152/japplphysiol.00803.2019 [PubMed: 32298211]
29. Gehr P, Bachofen M, Weibel ER. The normal human lung: ultrastructure and morphometric estimation of diffusion capacity. Respir Physiol. 1978;32(2):121–140. doi:10.1016/0034-5687(78)90104-4 [PubMed: 644146]
30. Weibel ER, Knight BW. A morphometric study on the thickness of the pulmonary air-blood barrier. J Cell Biol. 1964;21(3):367–396. doi:10.1083/JCB.21.3.367 [PubMed: 14189911]
31. Niedbalski PJ, Lu J, Hall CS, et al. Utilizing flip angle/TR equivalence to reduce breath hold duration in hyperpolarized 129Xe 1-point Dixon gas exchange imaging. Magn Reson Med. 2022;87(3):1490–1499. doi:10.1002/mrm.29040 [PubMed: 34644815]
32. Quanjer PH, Stanojevic S, Cole TJ, et al. Multi-ethnic reference values for spirometry for the 3–95-yr age range: The global lung function 2012 equations. European Respiratory Journal. 2012;40(6):1324–1343. doi:10.1183/09031936.00080312 [PubMed: 22743675]
33. Wang Z, He M, Bier E, et al. Hyperpolarized 129 Xe gas transfer MRI: the transition from 1.5T to 3T Magnetic Resonance in Medicine. Magn Reson Med. Published online 2018:2374–2383. doi:10.1002/mrm.27377
34. Wang Z, Robertson SH, Wang J, et al. Quantitative analysis of hyperpolarized 129 Xe gas transfer MRI. Med Phys. 2415;44(6). doi:10.1002/mp.12264
35. Wang Z, He M, Virgincar RS, Bier EA, Luo S, Driehuys B. Quantifying Hyperpolarized 129Xe Gas Exchange MRI Across Platforms, Field Strength, and Acquisition Parameters. In: ISMRM 27th Annual Meeting and Exhibition. ; 2019:#4139.
36. Fischbach FT. A Manual of Laboratory and Diagnostic Tests. 7th ed. Lippincott Williams & Wilkins; 2003.
37. Hahn AD, Kammerman J, Evans M, et al. “Repeatability of Regional Pulmonary Functional Metrics of Hyperpolarized 129Xe Dissolved Phase MRI.” J Magn Reson Imaging. 2019;50(4):1182. doi:10.1002/JMRI.26745 [PubMed: 30968993]
38. Stewart NJ, Horn FC, Norquay G, et al. Reproducibility of quantitative indices of lung function and microstructure from 129Xe chemical shift saturation recovery (CSSR) MR spectroscopy. Magn Reson Med. 2017;77(6):2107–2113. doi:10.1002/mrm.26310 [PubMed: 27366901]
39. Li H, Zhang Z, Zhao X, Sun X, Ye C, Zhou X. Quantitative evaluation of radiation-induced lung injury with hyperpolarized xenon magnetic resonance. Magn Reson Med. 2016;76(2):408–416. doi:10.1002/MRM.25894 [PubMed: 26400753]
40. Zhong J, Zhang H, Ruan W, et al. Simultaneous assessment of both lung morphometry and gas exchange function within a single breath-hold by hyperpolarized 129Xe MRI. NMR Biomed. 2017;30(8):e3730. doi:10.1002/NBM.3730
41. Zhang Z, Guan Y, Li H, et al. Quantitative comparison of lung physiological parameters in single and multiple breathhold with hyperpolarized xenon magnetic resonance. Biomed Phys Eng Express. 2016;2(5):055013. doi:10.1088/2057-1976/2/5/055013
42. Graham BL, Brusasco V, Burgos F, et al. 2017 ERS/ATS standards for single-breath carbon monoxide uptake in the lung. European Respiratory Journal. 2017;49(1). doi:10.1183/13993003.00016-2016
43. Wang JM, Robertson SH, Wang Z, et al. Using hyperpolarized 129Xe MRI to quantify regional gas transfer in idiopathic pulmonary fibrosis. Thorax. 2018;73(1):21–28. doi:10.1136/THORAXJNL-2017-210070 [PubMed: 28860333]
44. Wang Z, Bier EA, Swaminathan A, et al. Diverse cardiopulmonary diseases are associated with distinct xenon magnetic resonance imaging signatures. European Respiratory Journal. 2019;54(6). doi:10.1183/13993003.00831-2019

45. Bellemare F, Jeanneret A, Couture J. Sex differences in thoracic dimensions and configuration. Am J Respir Crit Care Med. 2003;168(3):305–312. doi:10.1164/rccm.200208-876OC [PubMed: 12773331]
46. Qing K, Tustison N, Altes T, et al. Gas Uptake Measures on Hyperpolarized Xenon-129 MRI are Inversely Proportional to Lung Inflation Level. In: ISMRM 23rd Annual Meeting and Exhibition. ; 2015:#1488.
47. Collier GJ, Chan HF, Stewart NJ, et al. Age and lung volume dependence of dissolved xenon-129 imaging parameters. In: Joint Annual Meeting ISMRM-ESMRMB 2022 and ISMRT Annual Meeting. ; 2022:#1174.
48. Grist JT, Chen M, Collier GJ, et al. Hyperpolarized 129Xe MRI abnormalities in dyspneic patients 3 months after COVID-19 Pneumonia. Radiology. 2021;301(1):E353–E360. doi:10.1148/radiol.2021210033 [PubMed: 34032513]
49. Ruppert K, Qian Y, Amzajerdian F, et al. Biases in Apparent Alveolar Septal Wall Thickness Measurements with Hyperpolarized Xenon-129 MRI Revealed by Numerical Simulations. In: American Thoracic Society International Conference Meetings Abstracts. American Thoracic Society; 2021:A4597. Accessed September 1, 2022. 10.1164/ajrccm-conference
50. REID JA, HEARD BE. The Capillary Network of Normal and Emphysematous Human Lungs Studied by Injections of Indian Ink. Thorax. 1963;18(3):201. doi:10.1136/THX.18.3.201 [PubMed: 14064613]
51. Ackermann M, Verleden SE, Kuehnel M, et al. Pulmonary Vascular Endothelialitis, Thrombosis, and Angiogenesis in Covid-19. New England Journal of Medicine. 2020;383(2):120–128. doi:10.1056/nejmoa2015432 [PubMed: 32437596]
52. Zanen P, van der Lee I, van der Mark T, van den Bosch JMM. Reference values for alveolar membrane diffusion capacity and pulmonary capillary blood volume. Eur Respir J. 2001;18(5):764–769. doi:10.1183/09031936.01.00232101 [PubMed: 11757625]
53. Crapo RO, Crapo JD, Morris AH. Lung tissue and capillary blood volumes by rebreathing and morphometric techniques. Respir Physiol. 1982;49(2):175–186. doi:10.1016/0034-5687(82)90072-X [PubMed: 7146650]
54. Stewart NJ, Parra-Robles J, Wild JM. Finite element modeling of (129)Xe diffusive gas exchange NMR in the human alveoli. J Magn Reson. 2016;271:21–33. doi:10.1016/J.JMR.2016.07.016 [PubMed: 27526397]
55. Ziegler AK, Grand J, Stangerup I, et al. Time course for the recovery of physical performance, blood hemoglobin, and ferritin content after blood donation. Transfusion (Paris). 2015;55(4):898–905. doi:10.1111/TRF.12926
56. Elzik ME, Dirschl DR, Dahners LE. Correlation of transfusion volume to change in hematocrit. Am J Hematol. 2006;81(2):145–146. doi:10.1002/AJH.20517 [PubMed: 16432852]
57. Kim KH, Oh KY. Clinical applications of therapeutic phlebotomy. J Blood Med. 2016;7:139. doi:10.2147/JBM.S108479 [PubMed: 27486346]
58. Mummy D, Swaminathan A, Bier E, et al. Hyperpolarized 129Xe MRI and spectroscopy in healthy control subjects reveals age-related changes in measurements of pulmonary gas exchange. In: Joint Annual Meeting ISMRM-ESMRMB 2022 and ISMRT Annual Meeting. ; 2022:#1168.
59. Ruppert K, Mata JF, Brookeman JR, Hagspiel KD, Mugler JP. Exploring lung function with hyperpolarized 129Xe nuclear magnetic resonance. Magn Reson Med. 2004;51(4):676–687. doi:10.1002/MRM.10736 [PubMed: 15065239]
60. Ladefoged J, Andersen AM. Solubility of Xenon-133 at 37°C in water, saline, olive oil, liquid paraffin, solutions of albumin, and blood. Phys Med Biol. 1967;12(3):353–358. doi:10.1088/0031-9155/12/3/307
61. Nijboer JMM, van der Horst ICC, Hendriks HGD, ten Duis HJ, Nijsten MWN. Myth or reality: Hematocrit and hemoglobin differ in trauma. Journal of Trauma - Injury, Infection and Critical Care. 2007;62(5):1310–1312. doi:10.1097/TA.0B013E3180341F54

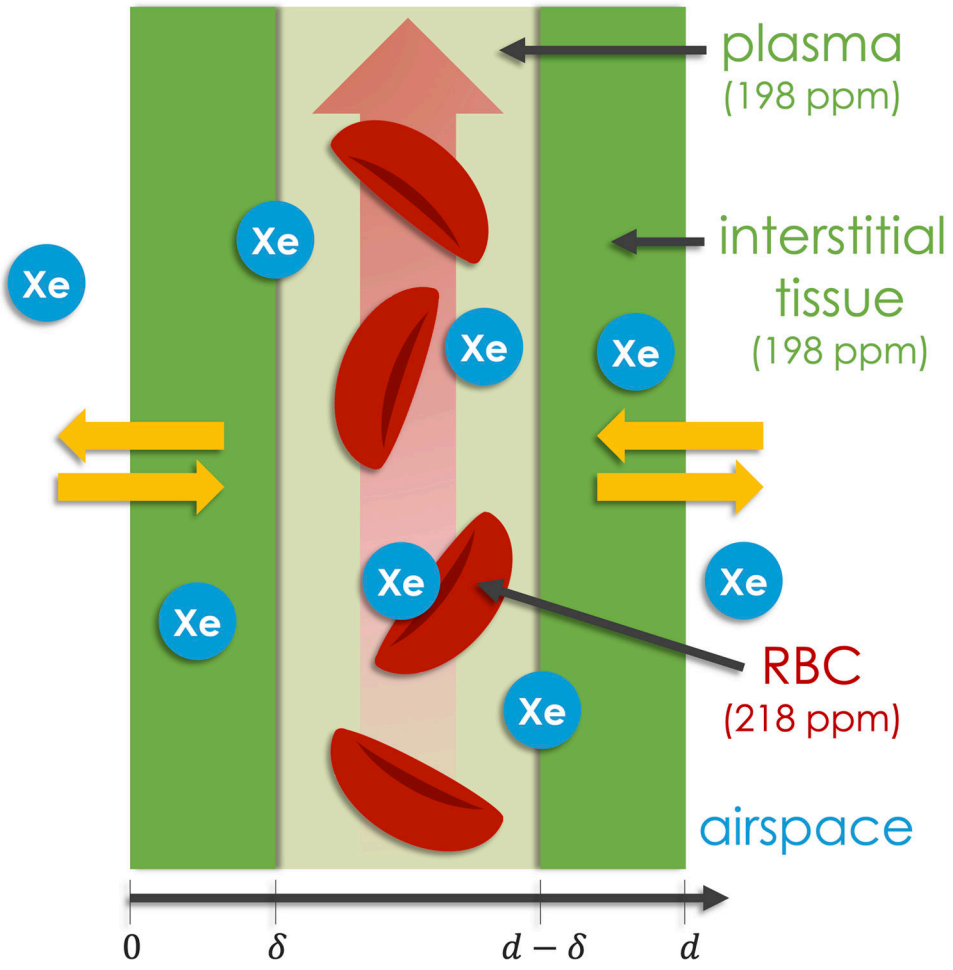

Figure 1.

The simplified lung microstructure assumed by MOXE, where the total width of the septum is d. The structure consists of two air-blood membranes of length δ, placed symmetrically on either side of the pulmonary capillary. ^{129}Xe diffuses in from the airspaces on either side, first entering the 198-ppm membrane compartment, which originates in the air-blood membranes and the plasma component of the blood. The atoms then reach the RBCs, which gives rise to the 218-ppm signal[20].

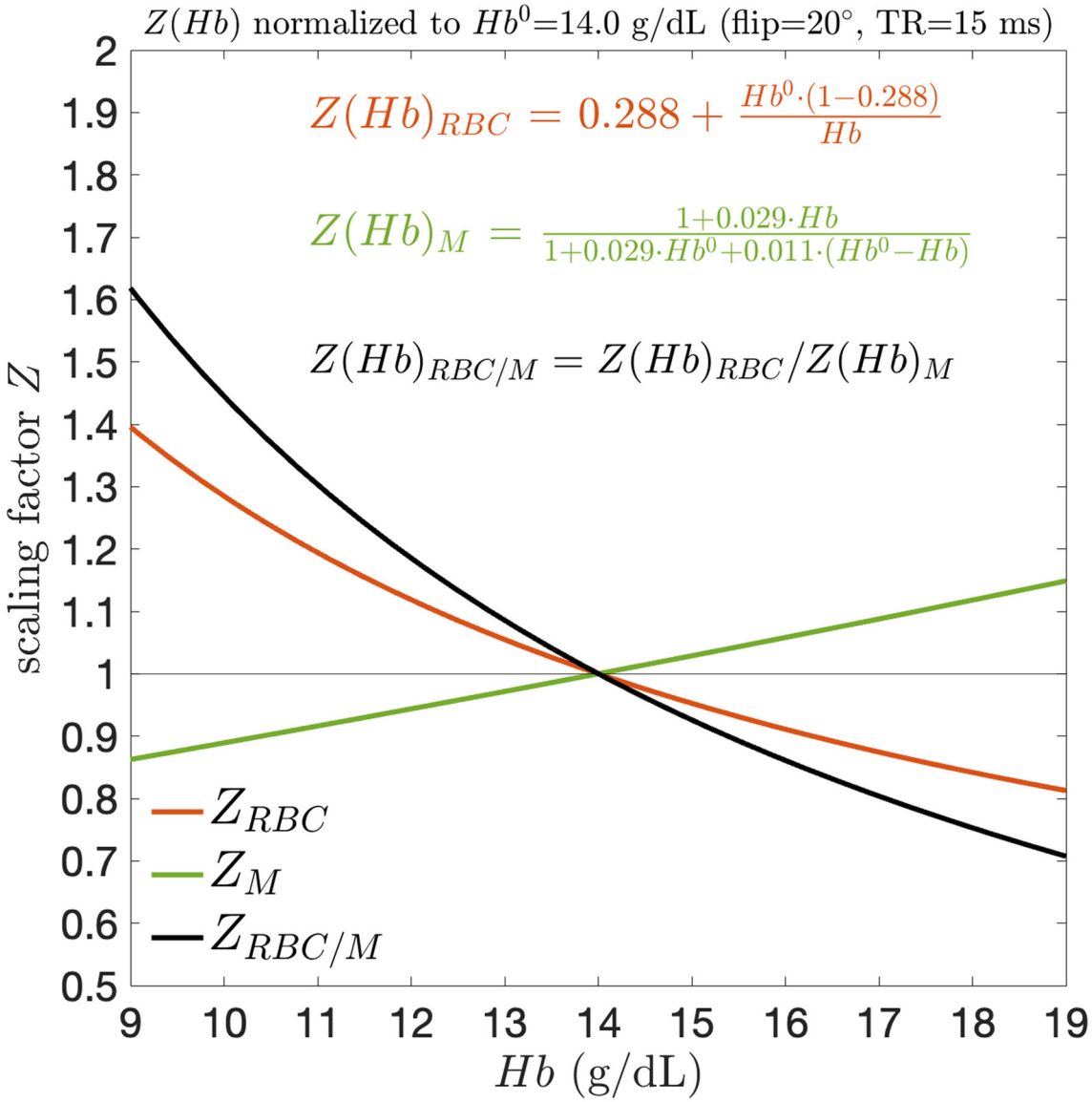

Figure 2.

Hb adjustment scaling factors (Z_M, Z_{RBC}, $Z_{RBC/M}$) as a function of systemic venous Hb. Within the typical Hb range, Z_M scales approximately linearly whereas the magnitude of Z_{RBC} and $Z_{RBC/M}$ is significantly larger at lower Hb than higher Hb.

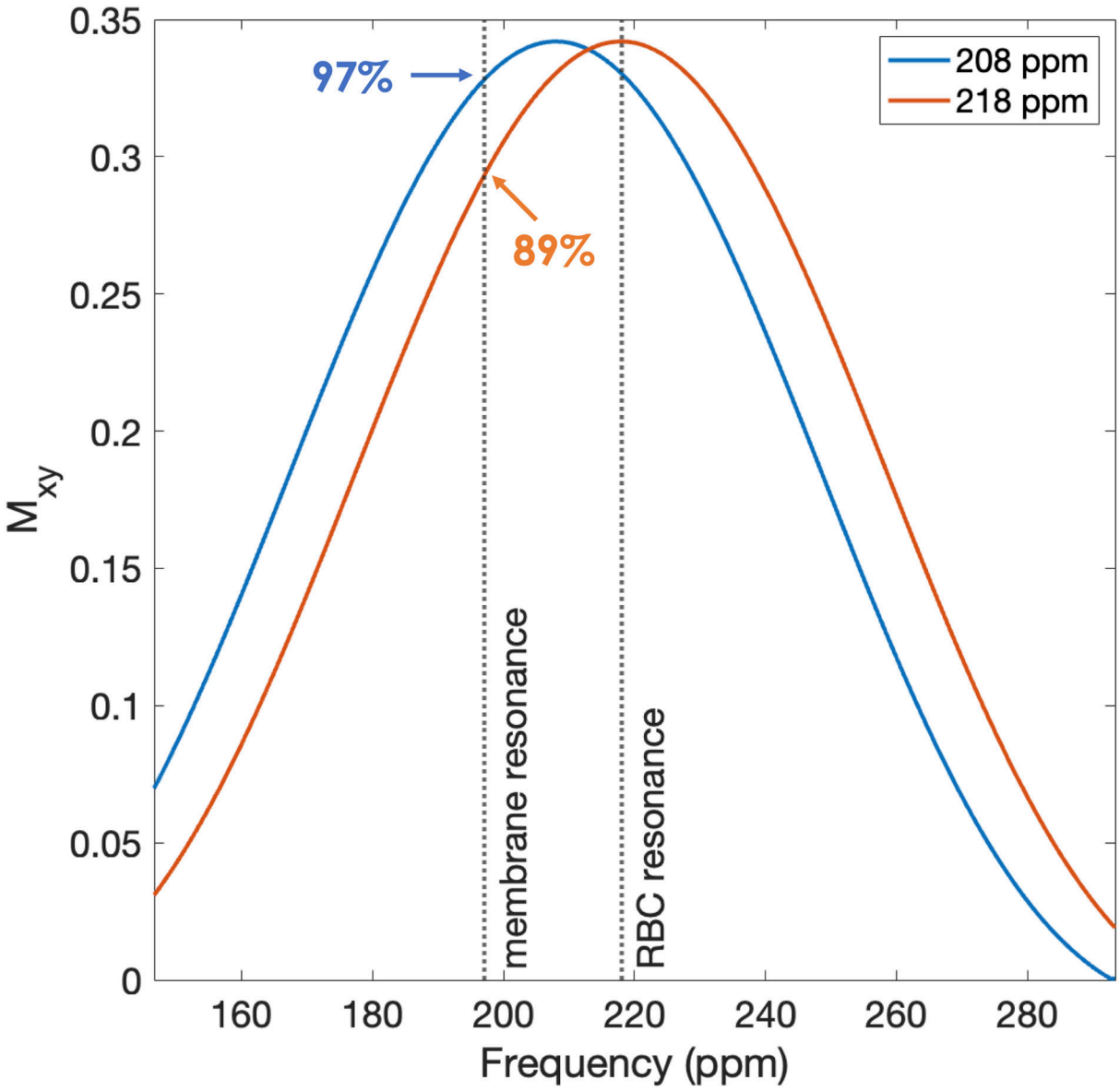

Figure 3.

Simulated distribution of transverse magnetization (M_{xy}) generated by 208- and 218-ppm Hanning-windowed sinc RF pulses. Vertical, dashed lines indicate the 198- and 218-ppm resonance frequencies corresponding to the chemical shifts of ^{129}Xe in membrane tissues and RBCs. Percentages show the magnitude of M_{xy} at the indicated point relative to the maximum M_{xy} plotted.

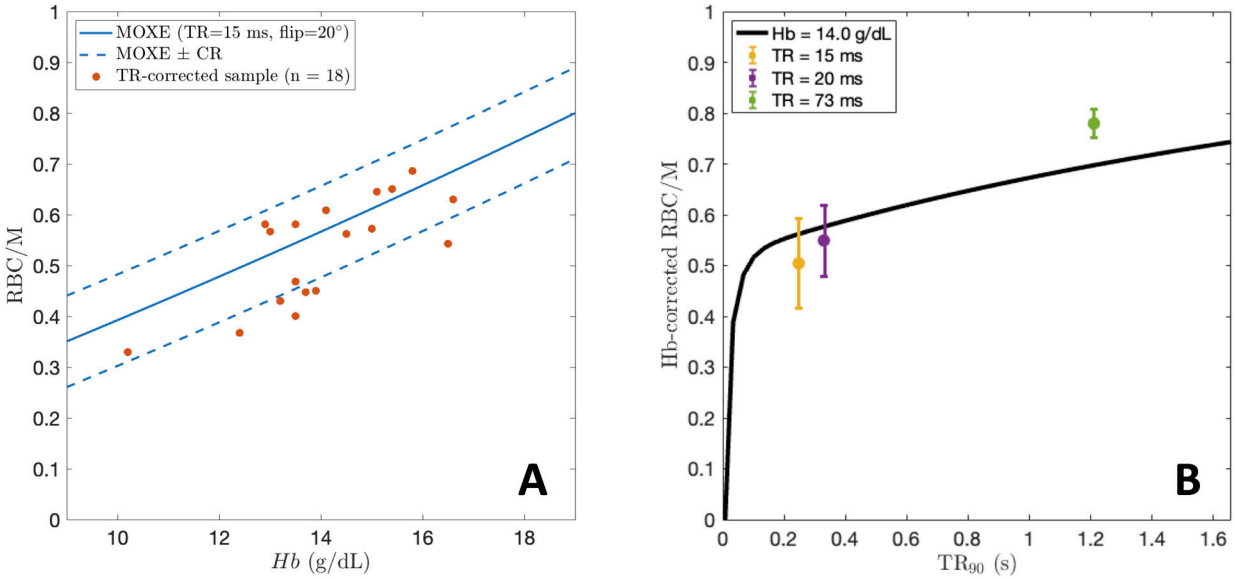

Figure 4.

A: Non Hb-adjusted RBC/M values at TR=15 ms and 20° flip from the healthy cohort plotted vs Hb, along with the MOXE-predicted curve. RBC/M from MOXE±CR for RBC/M is plotted over the data. B: Distributions of Hb-adjusted RBC/M values measured at three different TRs (15, 20, and 73 ms). The black line depicts the RBC/M curve predicted by MOXE at $Hb^0 = 14\text{g/dL}$.

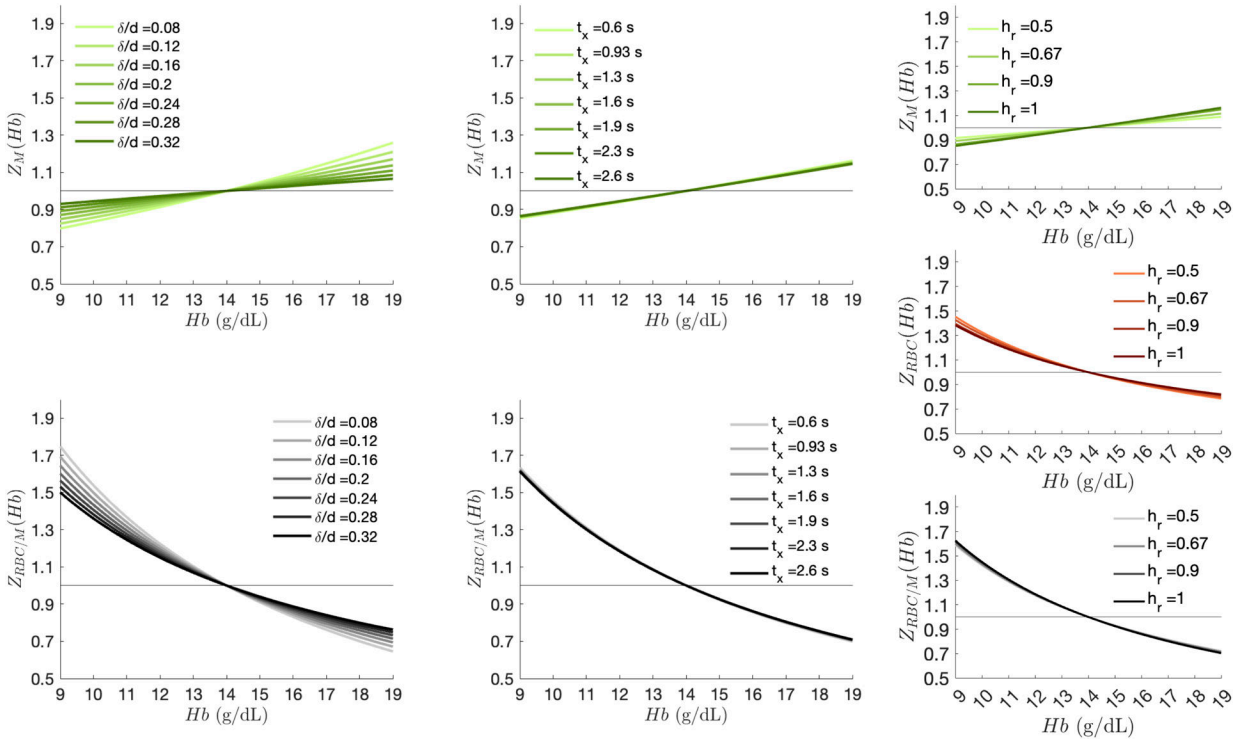

Figure 5.

Changes in Hb adjustment curves with respect to different δ/d, t_x, and h_r values. Adjustment factors vary minimally with changes in t_x and h_r but are sensitive to changes in δ/d, with higher ratios dampening the membrane and RBC/M Hb adjustment factors. Note, δ/d and t_x sensitivity plots are not shown for the RBC adjustment factors as Z_{RBC} is not dependent on these parameters.

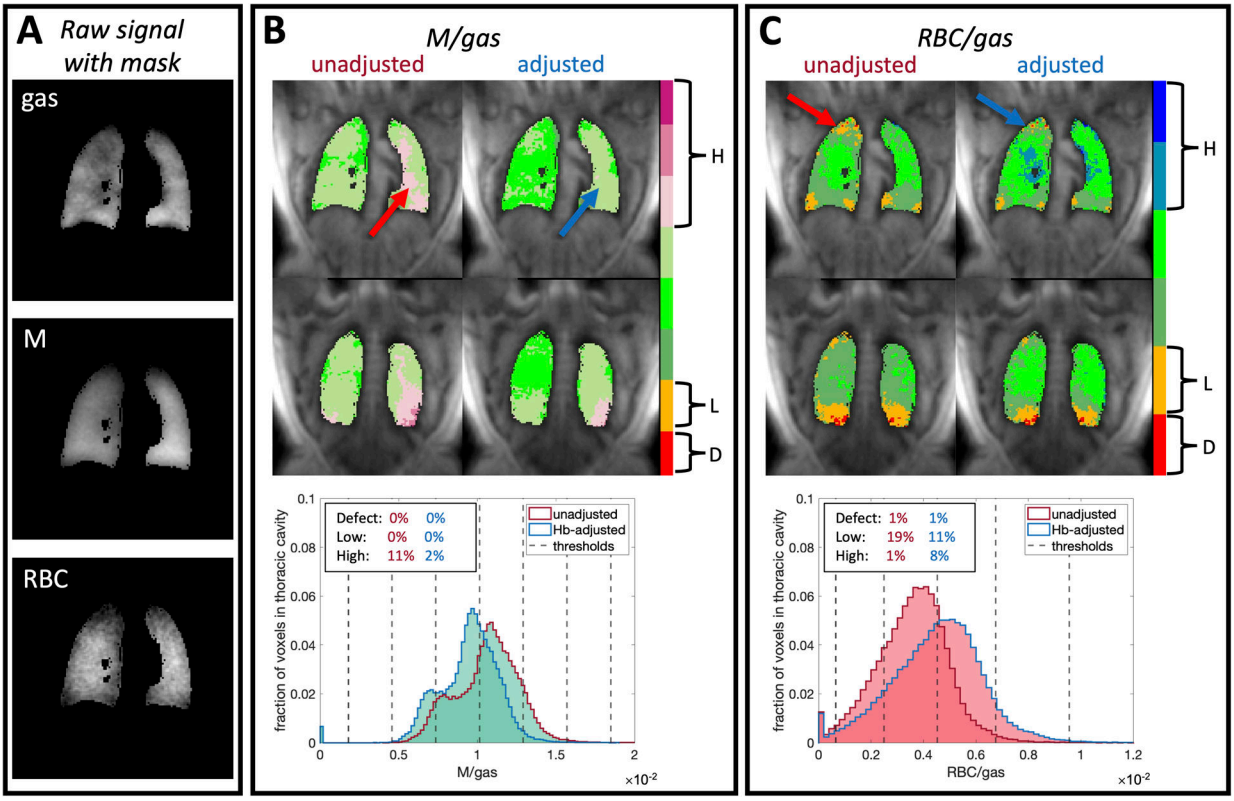

Figure 6.

Representative images of gas, M, and RBC after application of a thoracic cavity mask (A) for a healthy subject with Hb=10.2 g/dL along with the application of Hb adjustment factors to the 3D gas exchange maps of M/gas (B) and RBC/gas (C). We also show the changes in voxel intensity distributions and defect (D), low (L), and high (H) percentages along with the thresholds that define the color bins. The subject's low Hb causes membrane uptake to be over-estimated, while RBC transfer is underestimated. After adjusting the images to $Hb^0 = 14\text{g/dL}$, the apparent high membrane uptake decreases from 11% to 2%, while low RBC transfer decreases from 19% to 11%. Arrows indicate regions where particularly high membrane uptake and low RBC transfer are resolved after adjustment. Notably, this subject's RBC/M ratio increases by ~40% from 0.38 to 0.53 after adjustment.

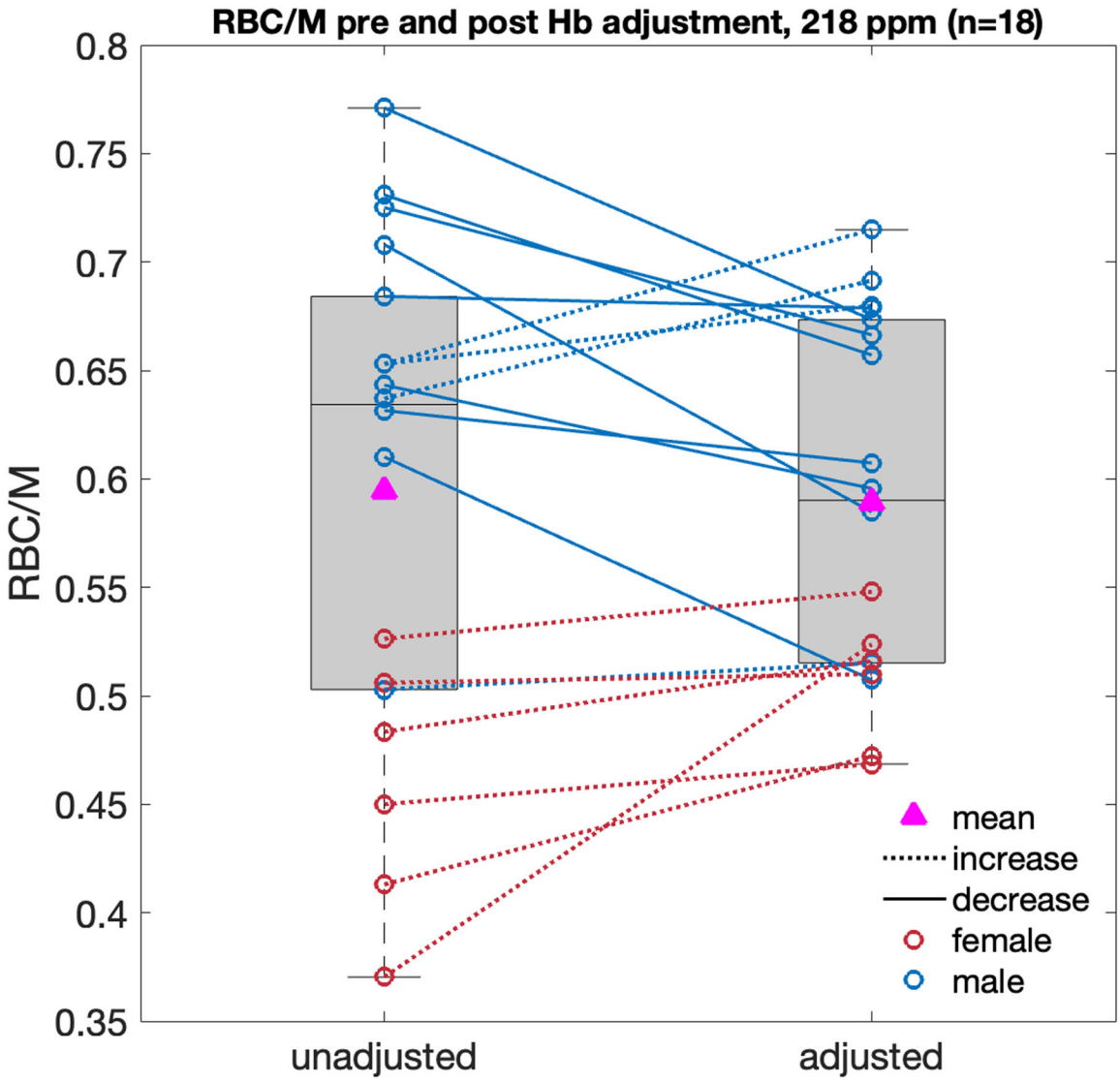

Figure 7.

Non Hb-adjusted and Hb-adjusted RBC/M ratios from the healthy young cohort (n=18, age=25.0±3.4 yrs) for dissolved-phase excitation at 218 ppm, TR=15 ms and 20° flip angle. RBC/M in the male sample was significantly higher than in the female sample both before adjustment (0.663±0.070 vs. 0.458±0.059, $p<0.0001$) and after (0.631±0.069 vs. 0.506±0.031, $p<0.001$). Applying subject-specific Hb adjustments causes the mean/SD of the total sample to change from 0.594±0.118 to 0.589±0.083.

Table 1.

Parameters used in the MOXE model, as determined from current literature for healthy populations.

Variable	Description	Literature value
$S_A/V_g\ (cm-1)$	Alveolar surface area to volume ratio[20]	250
$d\ (\mu m)$	Total septum thickness[28]	12
$\delta\ (\mu m)$	Air-blood membrane thickness[29]	2.22
$t_X\ (s)$	Capillary transit time[20]	1.6
$D\ (cm2/s)$	Diffusion coefficient of dissolved xenon[59]	3.3×10^{-6}
λ	Ostwald solubility of xenon in lung parenchyma[22]	0.2
λ_{RBC}	Ostwald solubility of xenon in RBCs[60]	0.19
λ_P	Ostwald solubility of xenon in plasma[60]	0.091
$Hb^0\left(g/dL\right)$	Healthy reference value for volume of venous hemoglobin[19]	14
h_r	Ratio of regional pulmonary Hct to venous Hct[25]	0.9
$a\ (dL/g)$	$h_r \cdot$ (Hct to Hb conversion factor[61])	$(0.9)\cdot(2.953\times10^{-2})$

Table 2.

Hb-adjusted RBC/M reference values (mean±SD) for dissolved-phase excitation at 208 and 218 ppm compared with values from age-matched healthy cohorts. Rescaled values have been adjusted for TR and flip angle in reference to TR=15 ms and flip=20°. Values from Bier et al. and Grist et al. have also been adjusted for unequal dissolved-phase excitation.

Reference	Flip angle	TR (ms)	Average age (yrs)	Sample size	Published RBC/M	Rescaled RBC/M
Xie et al. (2019)[16]	90°	100	25.8±1.5	4 (0 female)	0.47±0.06	0.51±0.07
Grist et al. (2021)[48]	40°	23	29.0±3.0	5 (5 female)	0.50±0.1	0.62±0.12
Bier et al. (2019)[6]	20°	20	26.3±5.0	8 (1 female)	0.59±0.12	0.52±0.11
This work RBC/M (208 ppm)	**20°**	**15**	**25.0±3.4**	**18 (6 female)**		**0.53±0.07**
This work RBC/M (218 ppm)	**20°**	**15**	**25.0±3.4**	**18 (6 female)**		**0.59±0.08**